Contrary neuronal recalibration in different multisensory cortical areas

Fu Zeng[1], Adam Zaidel[2,*] and Aihua Chen[1,*]

1. Key Laboratory of Brain Functional Genomics (Ministry of Education), East China Normal University, 3663 Zhongshan Road N., Shanghai 200062, China
2. Gonda Multidisciplinary Brain Research Center, Bar-Ilan University, Ramat Gan, 5290002, Israel

* Co-corresponding author.

Keywords:

cross-modal; plasticity; self-motion; vestibular; visual; adaptation

* Correspondence: ahchen@brain.ecnu.edu.cn (A.C.) or adam.zaidel@biu.ac.il (A.Z.)

In Brief:

The neural bases of multisensory plasticity are currently unknown. Here, Zeng et al. studied neuronal recalibration to a systematic visual-vestibular cue conflict. In multisensory cortical areas MSTd and PIVC, single-unit responses to visual and vestibular stimuli recalibrated to reduce the cue conflict, along with their respective unisensory perceptual shifts. By contrast, in higher-level VIP, both visual and vestibular neuronal responses recalibrated with vestibular perceptual shifts. This led to a surprising recalibration of visual responses opposite in direction to visual perceptual shifts. This exposes differential aspects of multisensory plasticity across multisensory cortical areas, and reveals a novel hybrid of visual responses within a vestibular reference frame in parietal neurons.

Highlights:

- In the presence of a systematic heading conflict, visual and vestibular cues recalibrate towards one another to reduce the conflict.
- In MSTd, neuronal responses to vestibular and visual cues recalibrated, each according to their respective cues' perceptual shifts.
- In PIVC, vestibular responses recalibrated according to vestibular perceptual shifts (cells were not visually tuned).
- In VIP, neuronal responses to both vestibular and visual cues recalibrated together with vestibular perceptual shifts (opposite in direction to visual perceptual shifts).
- Profound differences in neuronal recalibration expose different functions across multisensory cortical areas.

Abstract

The adult brain demonstrates remarkable multisensory plasticity by dynamically recalibrating information from multiple sensory sources. When a systematic visual-vestibular heading offset is experienced, the unisensory perceptual estimates recalibrate toward each other (in opposite directions) to reduce the conflict. The neural substrate of this recalibration is unknown. Here, we recorded single-neuron activity from the dorsal medial superior temporal (MSTd), parieto-insular vestibular cortex (PIVC), and ventral intraparietal (VIP) areas in three male rhesus macaques during visual-vestibular recalibration. Both visual and vestibular tuning in MSTd recalibrated - each according to their respective cues' perceptual shifts. Vestibular tuning in PIVC also recalibrated together with corresponding perceptual shifts (cells were not visually tuned). By contrast, VIP neurons demonstrated a unique phenomenon: both vestibular and visual tuning recalibrated according to vestibular perceptual shifts. Such that, visual tuning shifted, surprisingly, contrary to visual perceptual shifts. Therefore, while unsupervised recalibration (to reduce cue conflict) occurs in early multisensory cortices, higher-level VIP reflects only a global shift, in vestibular space.

Introduction

Our different sensory systems each continuously adapt to changes in the environment (Webster, 2012). Thus, to maintain stable and coherent perception in a multisensory and ever-changing world, the brain needs to dynamically adjust for sensory discrepancies between the different modalities. This process of multisensory recalibration takes place continually, and is perhaps more fundamental than multisensory integration because integration would not be beneficial when the underlying cues are biased. While the neural bases of multisensory integration have received a lot of attention (Chen et al., 2013a; Ernst and Banks, 2002; Ernst and Bülthoff, 2004; Ernst and Di Luca, 2011; Gu et al., 2008; Stein et al., 2014), the neural bases of multisensory recalibration have been explored to a much lesser degree.

Cross-modal recalibration has been observed in a variety of multisensory settings. One well-known example is the ventriloquist aftereffect (VAE), in which exposure to a consistent spatial discrepancy between auditory and visual stimuli induces a subsequent shift in the perceived location of sounds (Bertelson and De Gelder, 2004; Canon, 1970; Kramer et al., 2020; Radeau and Bertelson, 1974; Recanzone, 1998; Watson et al., 2021). Also, the rubber-hand illusion (RHI) leads to an offset in hand proprioception in the direction of the visually observed rubber hand (Abdulkarim et al., 2021; Botvinick and Cohen, 1998; Kennett et al., 2001; Thériault et al., 2022; Tsakiris and Haggard, 2005). Although it was initially thought that only the non-visual cues recalibrate to vision (visual dominance; (Brainard and Knudsen, 1993; Rock and Victor, 1964), further work in a variety of paradigms has revealed both visual and

non-visual recalibration (Atkins et al., 2003; Burge et al., 2010; Lewald, 2002; van Beers et al., 2002; Zaidel et al., 2011).

Most of what we know about multisensory recalibration is described at the behavioral level (Burge et al., 2008; Burge *et al.*, 2010; Lewald, 2002), with little known about its neuronal underpinnings. Recent EEG (Park and Kayser, 2021) and fMRI (Zierul et al., 2017) studies in humans have shed some light on this question. However, these methods lack the resolution to probe recalibration at the level of single neurons. A series of classic studies by Eric Knudsen and colleagues investigated multisensory plasticity at the neuronal and circuit levels, in the barn owl (Knudsen, 2002; Knudsen and Brainard, 1991; Linkenhoker and Knudsen, 2002). They found profound neuronal plasticity in juvenile owls reared with prismatic lenses that systematically displaced their field of view. In that case, the auditory space map in the optic tectum was recalibrated to be aligned with the displaced visual field (Knudsen and Brainard, 1991). However, multisensory plasticity is not limited to the development, and the neuronal bases of how multiple sensory systems continuously adapt to one another in the adult brain remain fundamentally missing.

Self-motion perception (the subjective feeling of moving through space) relies primarily on visual and vestibular cues (Butler et al., 2015; Butler et al., 2010; de Winkel et al., 2010; Fetsch et al., 2012; Fetsch et al., 2009; Gu et al., 2007; Warren et al., 1988). Multisensory integration of visual and vestibular signals can improve heading perception (Burge *et al.*, 2010; Butler *et al.*, 2015; Dokka et al., 2015; Gu *et al.*, 2008). However, conflicting or inconsistent visual and vestibular information often

93 leads to motion sickness (Oman, 1990; Reason and Brand, 1975). Interestingly, this
94 subsides after prolonged exposure to the sensory motion conflict, presumably through
95 brain mechanisms of multisensory recalibration (Held, 1961; Shupak and Gordon,
96 2006). Thus, self-motion perception – a vital skill for everyday function with intrinsic
97 plasticity – offers a prime substrate to study cross-sensory recalibration.

98 We previously investigated and found robust (behavioral) recalibration of both
99 visual and vestibular cues in response to a systematic vestibular-visual heading
100 discrepancy (Zaidel *et al.*, 2011). In that paradigm, no external feedback was given.
101 Thus, the need for recalibration arose solely because of the cue discrepancy (we
102 therefore call this condition *unsupervised*). The subjects (humans and monkeys)
103 recalibrated both visual and vestibular perceptual estimates by shifting them toward
104 each other, to reduce the conflict. This is in line with the notion that unsupervised
105 recalibration aims to maintain "internal consistency" between the cues (Burge *et al.*,
106 2010). However, the neuronal basis of this everyday multisensory plasticity is
107 unknown.

108 In a complementary behavioral study, we tested *supervised* self-motion
109 recalibration, by providing external feedback regarding cue accuracy (Zaidel et al.,
110 2013). There we found that supervised recalibration is a high-level cognitive process
111 that compares the combined-cue (multisensory) estimate to feedback from the
112 environment. This resulted in 'yoked' recalibration of both cues, in the same direction,
113 to reduce conflict between the combined estimate and external feedback. We
114 subsequently also investigated the neuronal substrate of *supervised* recalibration

(Zaidel et al., 2021). We found robust recalibration of both vestibular and visual neuronal tuning in the monkey ventral intraparietal (VIP) cortex, such that tuning for both cues shifted together, in accordance with the behavior. However, because in that paradigm both cues recalibrate in the same direction (yoking), neuronal tuning was also expected to shift in the same direction for both cues. Thus, differential aspects of neuronal recalibration for the individual cues could go undetected.

By contrast, in unsupervised recalibration, vestibular and visual cues shift in opposite directions (Zaidel *et al.*, 2011). Therefore, the unsupervised paradigm can better expose differences in the way that individual cues recalibrate to one-another in the brain. Because unsupervised recalibration occurs in the absence of external feedback, it is presumed to reflect implicit changes in perception. Thus, we expected to see its effects relatively early in the vestibular-visual integration hierarchy, and that these effects would propagate to higher-level areas. Unsupervised recalibration of single neurons in single behavioral sessions, has not been tested before. The resulting psychometric shifts are smaller (vs. supervised recalibration). Thus detecting its neuronal correlates is challenging, but imperative, to understand the neural bases of adult cross-sensory plasticity. Thus, the aim of this study was to test unsupervised recalibration of visual and vestibular neuronal tuning, and how it may differ across multisensory cortical areas.

Two relatively early multisensory cortical areas involved in self-motion perception are the medial superior temporal area (MSTd) and the parietal insular vestibular cortex (PIVC). Neurons in MSTd respond to large optic flow stimuli, conducive to the

visual perception of self-motion (Gu et al., 2006). Vestibular responses are also present in MSTd, however visual self-motion signals dominate (Gu *et al.*, 2008; Gu et al., 2012). PIVC has strong vestibular responses, without strong tuning to visual optic flow (Chen et al., 2010). Therefore, we expected to see perceptual shifts resulting from unsupervised calibration in MSTd and PIVC. Area VIP also has robust responses to visual and vestibular self-motion stimuli, however, it is marked by strong choice signals (Chen et al., 2016; Gu, 2018; Zaidel et al., 2017). It is thus considered a higher-level multisensory area involved in additional (currently not fully understood) cognitive functions. Different types of multisensory recalibration observed in these different multisensory areas can provide important insights into their differential underlying functions. Thus, in this study, we focused on these three multisensory cortical areas. We examined whether and how their visual and vestibular neural tuning changed in accordance with corresponding behavioral shifts during a single session (~1hr) of unsupervised cross-sensory recalibration.

Results

Three monkeys performed a task of heading discrimination in a paradigm that elicits unsupervised cross-sensory (vestibular-visual) recalibration. Simultaneous to behavioral performance, we recorded from single neurons extracellularly in areas MSTd (upper bank of the superior temporal sulcus, n=83: 19 from monkey D, 64 from monkey K), PIVC (upper bank and the tip of the lateral sulcus, n=160: 91 from monkey D, 69 from monkey B), and VIP (lower bank and tip of the intraparietal sulcus,

158 n=118: 103 from monkey D, 15 from monkey B). The paradigm followed the same
159 methodology as our previous behavioral study (Zaidel *et al.*, 2011). It consisted of
160 three consecutive blocks: pre-recalibration (**Fig. 1A**), recalibration (**Fig. 1B**), and
161 post-recalibration (**Fig. 1C**). We first (in the next section) present the monkeys'
162 perceptual recalibration results. Thereafter, we present the neural correlates thereof.

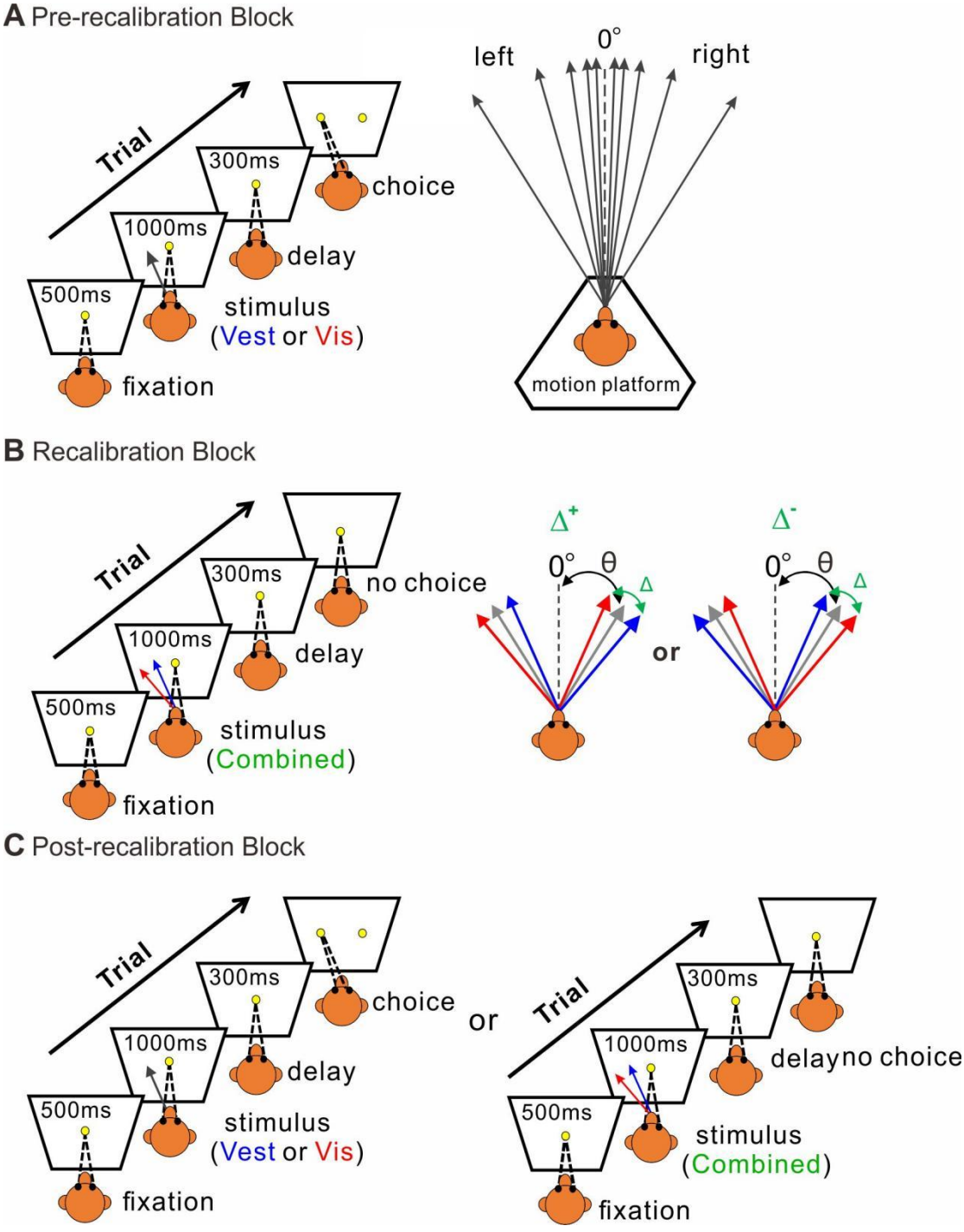

Figure 1. Multisensory recalibration paradigm. **(A)** Pre-recalibration block. The vestibular stimulus was provided by the motion platform (schematic on the right), and the visual stimulus was optic-flow simulation of self-motion (without motion of the platform) presented on a screen in front of the monkey (schematic on the left). The self-motion stimuli comprised linear motions (of either vestibular or visual stimuli) in a primarily forward direction, with slight deviations to the right or left (black arrows, schematic on the right). Monkeys were required to fixate on a central target (yellow circle) presented on the screen during the stimulus and then to report their perceived heading by making a saccade to one of two choice targets (left or right relative to straight ahead). **(B)** Recalibration block. Vestibular and visual stimuli were presented together ("combined") with a systematic discrepancy (Δ) between the vestibular and visual headings. The blue and red arrows represent the vestibular and visual headings, respectively. The gray arrows represent the combined cue headings (in between the vestibular and visual cues) and the black dashed lines represent straight ahead. **(C)** Post-recalibration block. The single-cue trials (like in A) were interleaved with combined-cue trials (like in B).

Both vestibular and visual cues recalibrate toward each other

Figure 2 shows example psychophysical data from two experimental sessions. Replicating our previous behavioral results (Zaidel *et al.*, 2011), we found that both visual and vestibular psychometric functions shifted in the direction required to reduce the cue conflict. Namely, when the vestibular and visual heading stimuli were systematically offset, such that they consistently deviated to the right and the left, respectively (Δ^{+}, **Fig. 2A**), the vestibular post-recalibration curve (blue) was shifted

rightward vs. pre-recalibration (black). Note that a rightward shift of the psychometric curve indicates a *leftward* perceptual shift (identified by a lower propensity for 'rightward' choices at 0° heading for the blue curve). Complementarily, the visual post-recalibration psychometric curve (red) shifted leftward vs. pre-recalibration (black), albeit to a lesser degree, indicating a *rightward* perceptual shift. In a reverse manner, when the vestibular and visual heading stimuli were offset to the left and right respectively (Δ^-, **Fig. 2B**), the vestibular post-recalibration curve (blue) shifted to the left, and the visual post-recalibration curve shifted to the right.

These behavioral shifts were quantified by the difference between the post- vs. pre-recalibration curves' PSEs (points of subjective equality). Each psychometric curve's PSE was detected by the heading at which it crosses y = 0.5 (marked by horizontal dashed lines in **Fig. 2**). The vestibular and visual psychometric shifts were: 3.40° and -1.01°, respectively in **Figure 2A**, and -3.68° and 1.00°, respectively, in **Figure 2B**. Thus, in both cases (**Fig. 2A, B**), both the vestibular and the visual cues shifted in the direction required to reduce the cue conflict (i.e. in opposite directions). Also, the vestibular shifts were larger (vs. visual).

These findings were consistent across sessions, as shown by the distributions of the vestibular and visual PSE shifts (solid bars for Δ^+ and striped bars for Δ^-) in **Figure 2C**. The vestibular PSEs were shifted significantly to the right for the Δ^+ condition (mean ± SE = 1.12° ± 0.12°; $p = 2.54 \times 10^{-15}$, paired t-test). And shifted significantly to the left for the Δ^- condition (mean ± SE = -1.76° ± 0.14°; $p = 1.77 \times 10^{-29}$, paired t-test). The visual PSEs were shifted significantly to the left for the Δ^+ condition (mean ± SE =

-0.73° ± 0.11°; $p = 1.60 \times 10^{-10}$, paired t-test). And shifted significantly to the right for the Δ^- condition (mean ± SE = 1.10° ± 0.10°; $p = 2.94 \times 10^{-21}$, paired t-test). Thus, consistent with our previous study, both cues shifted (in opposite directions) to reduce the cue conflict.

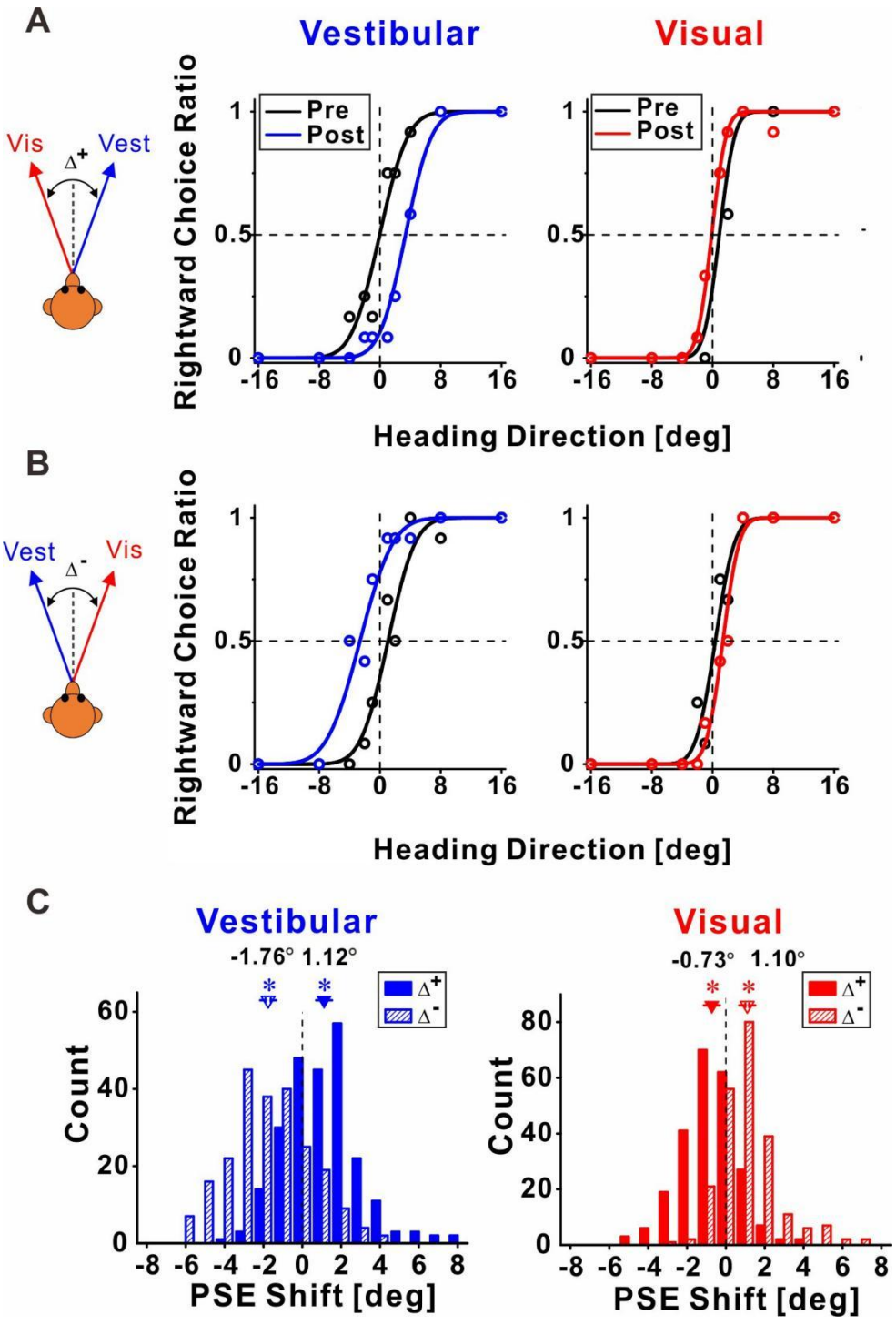

Figure 2. Multisensory recalibration behavior. (A, B) Example psychometric plots represent the ratio of the monkeys' rightward choices, as a function of stimulus heading direction. Data (circles) were fitted with cumulative Gaussian functions (solid lines). Pre-recalibration performance is presented for vestibular and visual cues (in the left and right columns, respectively) by the black curves. After recalibration, vestibular and visual cues were shifted (blue and red curves, respectively). Behavior for positive and negative delta (∆+ and ∆-, respectively) are presented in A and B, respectively. (C) Blue and red histograms represent the vestibular and visual PSE shift distributions, respectively. Solid and slash-textured histograms indicate positive and negative ∆, respectively. Inverted triangles (▼) and error bars represent mean SEM shifts. The numbers above triangles are the mean PSE shift. Asterisk symbols indicate significant shifts ($p < 0.05$). In vestibular cue, $p = 2.54 \times 10^{-15}$ for ∆+ condition, and $p = 1.77 \times 10^{-29}$ for ∆- condition, respectively. In visual cue, $p = 1.60 \times 10^{-10}$, n = 241 sessions for ∆+ condition, and $p = 2.94 \times 10^{-21}$, n = 227 sessions for ∆- condition, respectively, paired t-test.

Comparing the vestibular vs. visual shift magnitudes (using absolute values, pooled across Δ^+ and Δ^- conditions) demonstrated significantly larger vestibular vs. visual shifts (1.43° ± 0.09 and 0.91° ± 0.07°, respectively; $p = 3.40 \times 10^{-5}$, paired t-test). This result is also consistent with our previous study. Thus, the behavioral results from the original study (performed in the Angelaki laboratory) were replicated in these experiments (in the Chen laboratory) using a new set of monkeys, with simultaneous neuronal recording. In the following sections, we present how neuronal responses in areas MSTd, PIVC, and VIP (**Fig. 3**, **4,** and **5,** respectively) recalibrated in comparison

231 to the behavioral shifts.

232 ***Both vestibular and visual neuronal tuning in MSTd recalibrate with perceptual***
233 ***shifts***

234 Responses of an example neuron recorded from MSTd during unsupervised
235 recalibration are presented in **Figure 3A**. Behaviorally, the vestibular PSE shifted
236 rightward and the visual PSE shifted leftward (upper panel, **Fig. 3A**). Shifts in
237 neuronal tuning could be subtle, therefore we used neurometrics to expose and
238 quantify the neuronal shifts. Specifically, we calculated neurometric responses for the
239 heading stimuli using the neuron's firing rates and ROC analysis, and fit these with a
240 cumulative Gaussian function (for method details, see Gu et al., 2007). PSEs were
241 then extracted, similar to the psychometric curves. Neurometric curves for this
242 example neuron are presented in the third row of **Figure 3A**. For this MSTd neuron,
243 the vestibular neurometric shifted to the right, while the visual neurometric shifted to
244 the left. Thus, the shifts in vestibular and visual tuning were consistent with the
245 behavioral shifts.

246 Across the population (**Fig. 3B**) MSTd neuronal shifts were significantly
247 correlated with the behavioral shifts, both for vestibular and visual cues (r = 0.44, p =
248 0.038, N = 23, and r = 0.34, $p = 5.2 \times 10^{-3}$, N = 65, respectively; Pearson correlations).
249 Therefore, in area MSTd neuronal recalibration occurs in accordance with perceptual
250 recalibration, both for vestibular and visual cues.

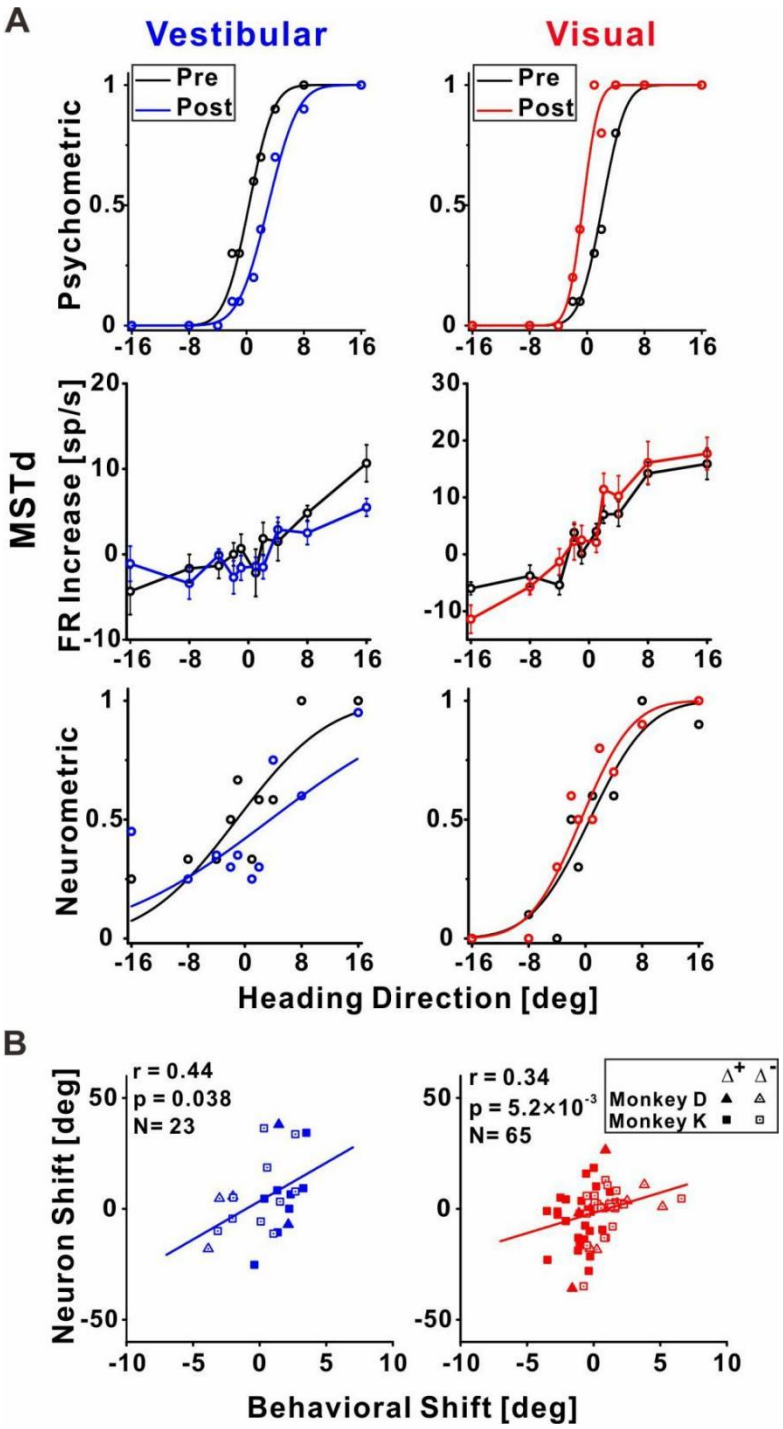

Figure 3. MSTd neuronal recalibration. (A) An example recalibration session (Δ^+) with simultaneous recording from MSTd. The top row depicts the behavioral responses, pre-, and post-recalibration. The vestibular psychometric curve shifted 3.01° (to the right) and the visual curve shifted -2.71° (to the left). Neuronal responses (second row) as a function of heading

(pre- and post-recalibration). Circles and error bars represent average firing rates (FRs, baseline subtracted) ± SEM. The third row shows corresponding neurometric functions with best-fitting cumulative Gaussian functions. The vestibular neuronal shift was 4.73° (to the right) and the visual neuronal shift was -1.22° (to the left). **(B)** Correlations between neuronal PSE shifts and behavioral PSE shifts for the vestibular and visual cues (left and right, respectively). Only cells with significant tuning ($p < 0.05$, Pearson correlation between firing rate and heading) in either pre- or post-recalibration blocks were included here. Solid symbols represent ∆+ and open symbols represent ∆-. The solid lines illustrate the regression lines of the data. $p = 0.038$, $n = 23$ neurons for vestibular cue, $p = 5.2 \times 10^{-15}$, $n = 65$ neurons for visual cue, Pearson correlation.

Vestibular neuronal tuning in PIVC recalibrates with perceptual shifts

In PIVC, a similar result was observed for vestibular tuning. The example vestibular neurometric curve **(Fig. 4A**, bottom left) shifted to the right, which was consistent with the behavioral shift **(Fig. 4A**, top left). Across the population of PIVC neurons, a significant positive correlation was seen between the neuronal and behavioral shifts for the vestibular cue ($r = 0.61$, $p = 1.26 \times 10^{-5}$, $N = 44$, Pearson correlation; **Fig. 4B**, left panel).

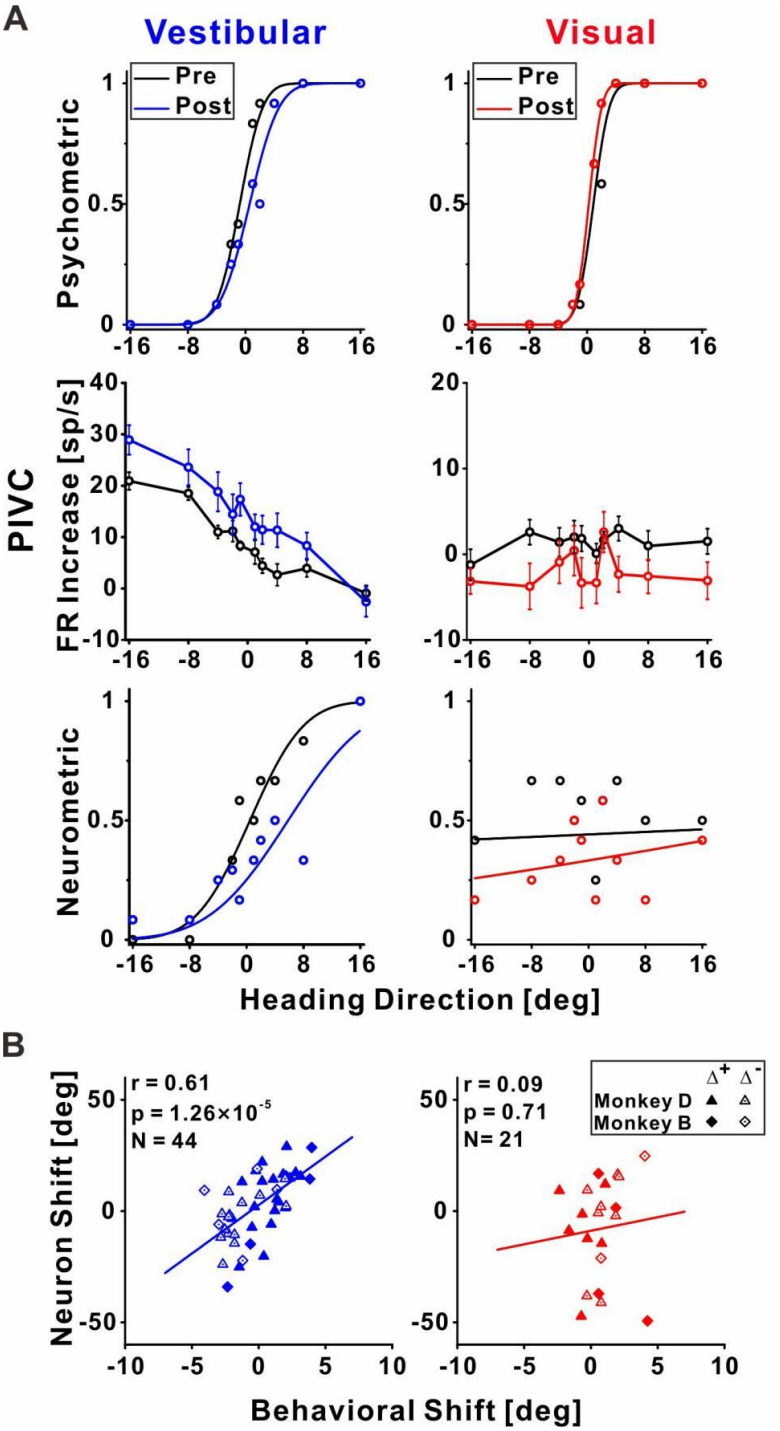

Figure 4. PIVC neuronal recalibration. (A) An example recalibration session (Δ^+) with simultaneous recording from PIVC (conventions are the same as **Figure 3**). The vestibular and visual psychometric curves shifted 1.37 and -0.51 (to the right and left, respectively). The vestibular neurometric curve shifted 5.37° (to the right). **(B)** Correlations between neuronal

PSE shifts and behavioral PSE shifts for the vestibular and visual cues. $p = 1.26 \times 10^{-5}$, n = 44 neurons for vestibular cue, p = 0.71, n = 21 neurons for visual cue, Pearson correlation.

In terms of visual tuning, this example neuron (and the other PIVC neurons) did not demonstrate robust visual responses (**Fig. 4A**, middle right). However, we still applied the same neurometric analysis for visual responses, using PIVC neurons that passed the significance criterion for visual tuning (albeit weak). No significant correlation was seen between the neuronal and behavioral shifts for the visual cue (r=0.09, p=0.71, N=21, Pearson correlation). Thus, in PIVC, the primary cortical region involved in vestibular function, neuronal tuning shifts were consistent with perceptual shifts, for the vestibular cue.

Vestibular and visual neuronal tuning in VIP both follow vestibular perceptual shifts

Figure 5A presents an example neuron from VIP. For the vestibular cue, the neuronal tuning curve shifted rightward (**Fig. 5A**, bottom left), in accordance with the vestibular behavioral shift (**Fig. 5A**, top left). Surprisingly, the visual neurometric curve also shifted rightward (**Fig. 5A**, bottom right). This was unexpected because the visual psychometric curve shifted leftward (**Fig. 5A**, top right). Thus, while the vestibular and visual behavioral psychometric curves shifted in opposite directions (toward each other) the vestibular and visual neurometric curves shifted together, in accordance with the vestibular (not visual) behavioral shift.

296 Across the population of VIP neurons, the vestibular neurometric shifts were
297 significantly positively correlated with the vestibular behavioral shifts (r = 0.69, p =
298 1.68× 10^{-8}, N = 53, Pearson correlation; **Fig. 5B**, left). Like in MSTd and PIVC, the
299 positive correlation coefficient indicates that neuronal and behavioral curves shifted in
300 the same direction for the vestibular cue. By contrast, the visual neurometrics in VIP
301 shifted in the opposite direction to the visual behavioral shifts. At the population level
302 neuronal and behavioral shifts for the visual cue were negatively correlated (r = -0.45,
303 p = 1.75 × 10^{-4}, Pearson correlation, N = 66; **Fig. 5B**, right). This exposes a striking
304 mismatch between visual neuronal responses in VIP and visual perceptual function. It
305 also exposes a striking mismatch between visual tuning in MSTd (which shifted in the
306 same direction as visual perception) vs. VIP (which shifted contrary to visual
307 perception).

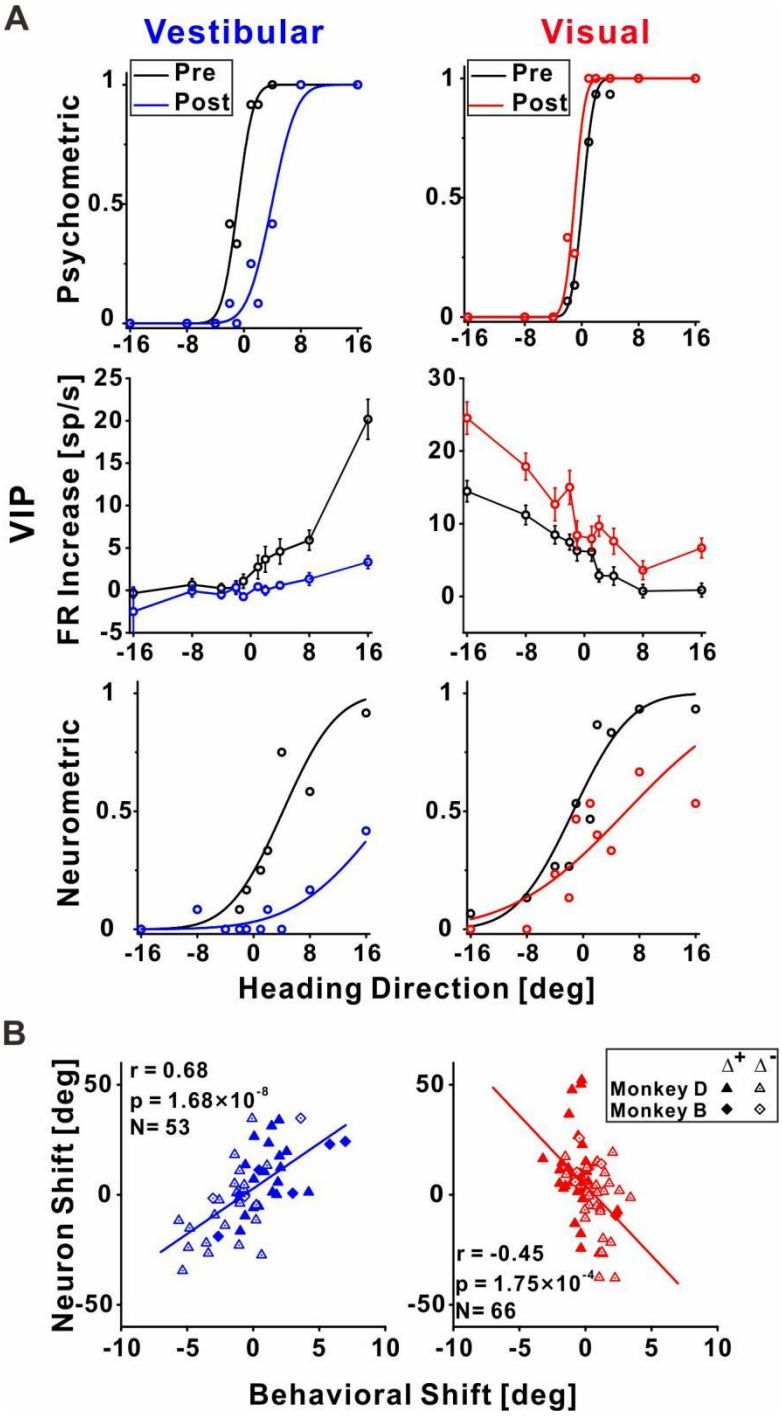

308 **Figure 5. VIP neuronal recalibration. (A)** An example recalibration session (Δ^+) with
309 simultaneous recording from VIP (conventions are the same as **Figure 3**). The vestibular and
310 visual psychometric curves shifted 4.81° and -1.13 (to the right and left, respectively). The
311 vestibular and visual neurometric curves shifted 15.18° and 7.58°, respectively (both to the

312 right). **(B)** Correlations between neuronal PSE shifts and behavioral PSE shifts for the
313 vestibular and visual cues. $p = 1.68 \times 10^{-8}$, n = 53 neurons for vestibular cue, $p = -0.45 \times 10^{-4}$,
314 n = 66 neurons for visual cue, Pearson correlation.

315 To test whether this mismatch between behavior and tuning for visual cues in VIP
316 relates to specific subtypes of neurons, we sorted the VIP data into three subsets:
317 neurons with multisensory (vestibular and visual) responses, and two groups with
318 unisensory (only vestibular or only visual) responses (**Supplemental Fig. 1A**). Similar
319 results were seen for both multisensory and unisensory neurons (the
320 neuronal-behavioral correlations remained consistently positive and negative for
321 vestibular and visual cues, respectively). We further sorted the multisensory neurons
322 into those with congruent and opposite vestibular and visual heading preferences
323 (Chen et al., 2011b; Gu *et al.*, 2006) with no observable differences (**Supplemental**
324 **Fig. 1B**). Therefore, the contrary shifts of visual tuning in VIP seem to reflect a general
325 feature of this cortical area, rather than an anomaly of a subgroup of neurons.

326 ***Temporal evolution of the correlation between neuronal and behavioral shifts***

327 The tuning curves in **Figures 3–5** were calculated using mean firing rates
328 averaged across the stimulus duration. But the self-motion stimuli generated by the
329 platform and optic flow followed a specific dynamical time-course, specifically, a
330 Gaussian velocity profile and correspondingly a biphasic acceleration profile (see
331 bottom row, **Fig. 6**). Therefore, we further examined whether the correlations between

behavioral recalibration and shifts in neuronal tuning depend on the time point within the stimulus interval.

For MSTd neurons, positive correlations (between behavioral and neuronal shifts) were seen for both vestibular and visual cues during the stimulus (**Fig. 6A**). The profile of correlations followed the velocity profile closely. Namely correlations increased toward the middle of the stimulus, and dropped off rapidly at the end of the stimulus. Significant correlations (blue and red asterisk markers for vestibular and visual cues, respectively) were only seen around the middle of the stimulus. Thus neural recalibration in MSTd (is accordance with behavioral recalibration) is seen in velocity responses, which are transient (evident only during the stimulus).

For PIVC neurons, positive correlations (between behavioral and neuronal shifts) were seen only for vestibular cues, during the stimulus (**Fig. 6B**). Like MSTd, the correlations seemed to follow the velocity profile of the stimulus, with significant values around the middle of the stimulus (upper panel in **Fig. 6B**). Correlations in the visual condition were very weak and not significant (middle panel in **Fig. 6B**).

A very different profile was seen in VIP. Firstly, as described above, correlations between neuronal and behavioral recalibration were positive for the vestibular cue (upper panel in **Fig. 6C**) and negative for the visual cue (middle panel in **Fig. 6C**). Furthermore, the time-course of these correlations was different in VIP: they increased in size gradually (positively for vestibular and negatively for visual), reaching a maximum around the middle of the stimulus epoch (the velocity peak), but then remained elevated beyond the end of the stimulus (**Fig. 6C**). This pattern is in

line with sustained neuronal activity described previously for VIP. However, here this sustained activity correlated with subsequent vestibular choices, and was contrary to visual choices. Thus the sustained activity is not generically choice related, but rather in accordance with recalibrated vestibular function.

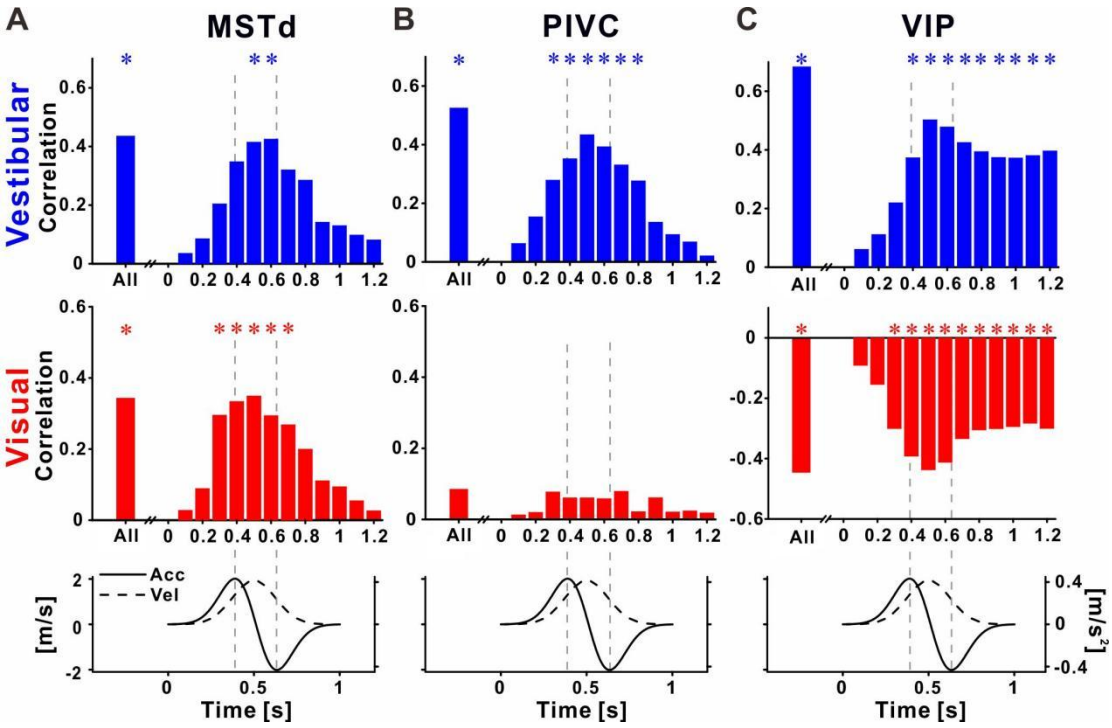

Figure 6. Recalibration of neuronal responses within the stimulus time-course. Correlations between neuronal and behavioral PSE shifts, using the neuronal activity at specific time-points during the stimulus, for **(A)** MSTd, **(B)** PIVC, and **(C)** VIP. Top row: vestibular (blue histograms), second row: visual (red histograms), third row: stimulus (acceleration and velocity) time-course. Vertical dashed lines mark the acceleration peaks, and '*' symbols mark significant correlations. Pearson correlation.

364 ***VIP choice signals are reduced during cross-sensory recalibration***

365 Previous studies have found that neuronal responses in VIP are strongly
366 influenced (perhaps even dominated) by choice signals (Chen et al., 2021; Zaidel *et*
367 *al.*, 2017). Hence our finding here, that neuronal tuning recalibrated contrary to
368 behavioral shifts for the visual cue, was surprising and counterintuitive. We therefore
369 wondered what happened to the strong choice signals for which VIP is renowned,
370 which would predict that neuronal tuning (also for visual cues) would shift with
371 behavior. To visualize choice tuning for an example VIP neuron, we plotted
372 'choice-conditioned' tuning curves, namely, neuronal responses as a function of
373 heading, separately for rightward and leftward choices, (**Fig. 7**). In the
374 pre-recalibration block vestibular responses were strongly choice related (**Fig. 7A**, left
375 plot) – neuronal responses to the same heading stimulus were larger when followed
376 by rightward (►, dark blue) vs. leftward (◄, cyan) choices (the dark blue line lies
377 above the cyan line). After recalibration, the choice effect decreased (**Fig. 7A**, right
378 plot) – the choice-conditioned tuning curves were no longer separate. Similarly, visual
379 responses were strongly choice-related pre-recalibration, and this decreased
380 post-recalibration (**Fig. 7B**). To quantify the choice (and sensory) components of
381 neuronal activity, and to observe how these changed after recalibration, we applied a
382 partial correlation analysis (Zaidel *et al.*, 2017). For this example neuron, the partial
383 choice correlation values (R_c, presented on the plots) were reduced both for vestibular
384 and visual cues.

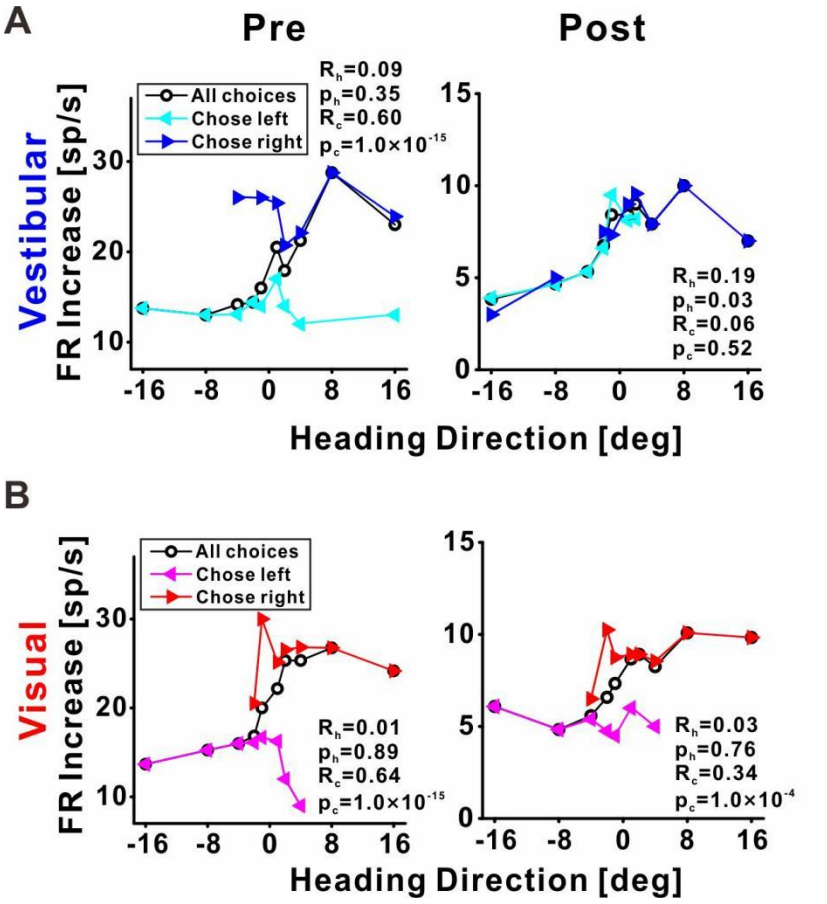

385 **Figure 7. Choice tuning is reduced post-recalibration in an example VIP neuron.**
386 Neuronal responses for example VIP neuron to **(A)** vestibular and **(B)** visual heading stimuli,
387 pre- and post-recalibration (left and right columns, respectively). Blue and cyan curves depict
388 choice-conditioned tuning curves (neuronal responses followed by rightward and leftward
389 choices, respectively) for the vestibular cue. Red and magenta curves depict
390 choice-conditioned tuning curves for the visual cue. Black curves (in the corresponding plots)
391 represent all responses (not sorted by choice). Partial heading (R_h) and partial choice (R_c)
392 correlations (with corresponding p-values) are presented on the plots.

393 Across our sample of VIP neurons, the choice partial correlations in the
394 post-recalibration block were significantly reduced compared to the pre-recalibration

block, for both vestibular (p = 3.73 × 10^{-3}, paired t-test) and visual (p = 4.39 × 10^{-3}, paired t-test; **Fig. 8B**) cues. However, the heading partial correlations (R_h) did not differ significantly from pre- to post-recalibration, neither for vestibular (p = 0.36, paired t-test) nor visual (p = 0.47, paired t-test; **Fig. 8A**) cues. For these statistical comparisons and for plotting we used the squared partial correlations (which quantify the amount of unique variance explained by choice or heading). We did not observe any changes in partial correlations in areas PIVC and MSTd (**Supplemental Fig. 2**). Lastly, there was no evidence for differences between post- and pre-recalibration baseline firing rates in any of the three areas (**Supplemental Fig. 3**; Bayes Factors (BF_{10}) presented on the corresponding subplots). Thus, shifts in neuronal tuning are not explained by changes in baseline activity.

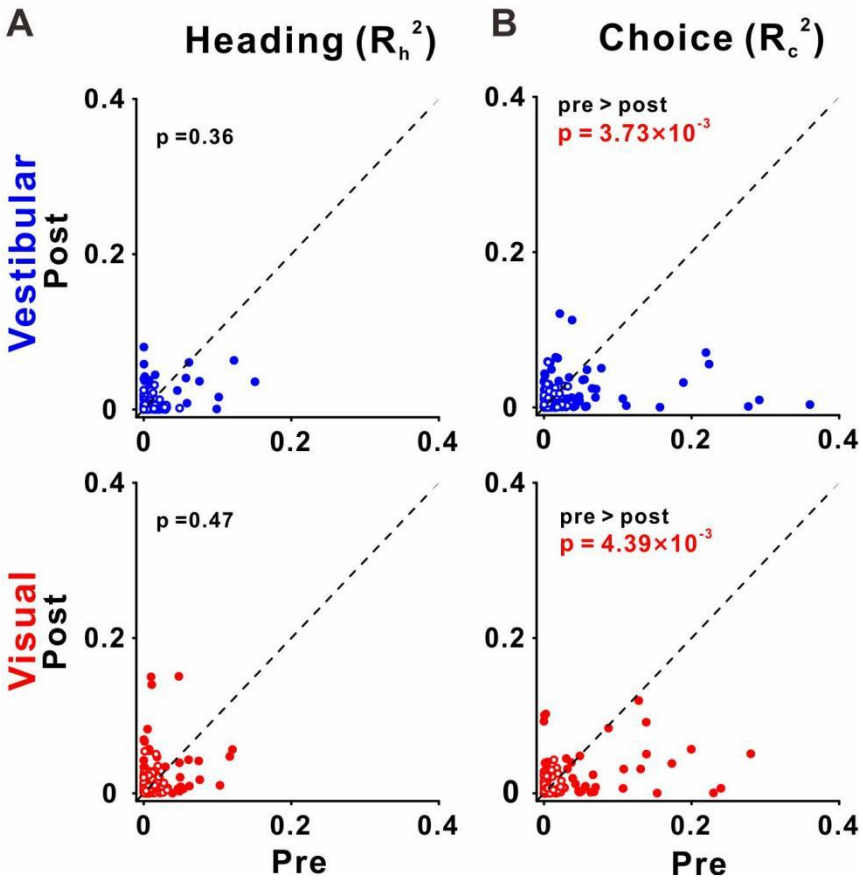

406 **Figure 8. Choice tuning is reduced in VIP post-recalibration. (A)** Heading and **(B)** choice
407 partial correlation coefficients (squared) are depicted post- vs. pre-recalibration. Blue and red
408 dots (top and bottom row) represent vestibular and visual cues, respectively. P-values for the
409 hypothesis of greater pre- vs. post-recalibration values are presented on the corresponding
410 plots. Paired t-test.

411 ## Discussion

412 This study provides the first demonstration of unsupervised (cross-sensory)
413 neuronal recalibration, in conjunction with behavioral recalibration, in single sessions.
414 Single-neurons from MSTd, PIVC, and VIP revealed clear but different patterns of
415 recalibration. In MSTd, neuronal responses to vestibular and visual cues recalibrated -
416 each according to their respective cues' perceptual shifts. In PIVC, vestibular tuning
417 similarly recalibrated together with the corresponding vestibular perceptual shifts (the
418 PIVC cells were not robustly tuned to visual stimuli). However, recalibration in VIP was
419 notably different: both vestibular and visual neuronal tuning recalibrated in the
420 direction of the vestibular perceptual shifts. Thus, visual neuronal tuning shifted,
421 surprisingly, contrary to visual perceptual shifts. These results indicate that neuronal
422 recalibration differs profoundly across multisensory cortical areas.

423 ### Neural correlates of vestibular-visual recalibration

424 To investigate the neuronal bases of unsupervised cross-sensory recalibration,
425 we first replicated the behavioral results from our previous study (Zaidel *et al.*, 2011).

Indeed, in the presence of a systematic vestibular-visual heading offset (with no external feedback) vestibular and visual cues both recalibrated in the direction required to reduce the cue conflict. And, as before, the vestibular shifts were larger compared to the visual shifts. Thus we confirmed robust recalibration of vestibular and visual cues, resulting from a systematic discrepancy between the cues' headings in an unsupervised context (i.e., without external feedback).

Since there was no external feedback regarding which cue was (in)accurate, unsupervised recalibration is driven by the cue conflict, presumably through an internal mechanism to maintain consistency between vestibular and visual perceptual estimates (Zaidel *et al.*, 2011). Accordingly, we expected to see neuronal correlates of perceptual recalibration in early multisensory areas related to self-motion perception, specifically: MSTd, which primarily responds to visual (but also vestibular) self-motion stimuli, and PIVC, which primarily responds to vestibular stimuli. We further expected that the neuronal recalibration in MSTd and PIVC would propagate to higher-level multisensory area VIP.

In MSTd, we indeed found that both visual and vestibular neuronal signals recalibrated, each in accordance with their corresponding cue's behavioral shifts. Hence, recalibration of visual self-motion responses was observed at least at the level of MSTd, which is the primary area in the visual hierarchy to respond to large field optic flow stimuli (Britten, 2008; Britten and van Wezel, 1998; 2002; Duffy and Wurtz, 1995; Gu *et al.*, 2008; Gu *et al.*, 2012; Gu *et al.*, 2006; Wurtz and Duffy, 1992). We cannot ascertain whether recalibration to visual responses occurred already in earlier

448 visual regions, such as the middle temporal visual area (MT), which projects to MSTd
449 (Maunsell and van Essen, 1983; Ungerleider and Desimone, 1986), or whether it
450 occurred only at the level of MSTd. Because MSTd is mainly a visual area, the
451 recalibration of vestibular signals observed in MSTd likely occurred in upstream
452 vestibular areas that project to MSTd, such as PIVC (Chen *et al.*, 2010; 2011a).
453 Indeed, robust vestibular recalibration (that was in line with the vestibular behavioral
454 shifts) was observed in PIVC. Hence, neuronal correlates of perceptual recalibration
455 were observed in relatively early multisensory areas related to self-motion perception
456 (MSTd and PIVC).

457 **Individualized recalibration of vestibular and visual cues**

458 Results from this experiment exposed individualized (sensory-specific) neuronal
459 recalibration (in MSTd and PIVC). Namely, visual and vestibular tuning curves shifted
460 differently (in opposite directions). This provides neuronal evidence against 'visual
461 dominance', even for short-term recalibration (in single sessions). Rather, it supports
462 the idea that cross-sensory neuronal recalibration occurs also for visual (and not only
463 for non-visual) cues.

464 Furthermore, sensory-specific recalibration of visual and vestibular tuning implies
465 that the brain has mechanisms to separately monitor and recalibrate individual cues.
466 Cue-specific shifts in neuronal tuning were not seen during supervised recalibration,
467 because the cues largely shift together, in response to external feedback (Zaidel *et al.*,
468 2021). Even though in the supervised condition both unsupervised and supervised

shifts are in operation (superimposed, Zaidel et al. 2013), the supervised (yoked) component is large and dominates, thereby obscuring the individualized (unsupervised) shifts. Here, without external feedback, we were able to detect individualized shifts of the different cues, not previously observed. This exposes neuronal mechanisms to maintain internal consistency between vestibular and visual cues. This dynamic cross-sensory plasticity may underlie our adept ability to adapt to sensory conflict commonly experienced in many modes of transport (on land, at sea, or in flight).

Contrary recalibration in higher-level area VIP

VIP is a higher-level multisensory area (Bremmer et al., 2002; Colby et al., 1993; Duhamel et al., 1998; Schlack et al., 2002; Schlack et al., 2005; Schroeder and Foxe, 2002) with clear vestibular and visual heading selectivity (Chen *et al.*, 2011a; b). But the nature of these self-motion signals in VIP is not fully understood. In contrast to our prediction that recalibrated signals in MSTd and PIVC would simply propagate to VIP, we found a different and unexpected pattern of recalibration in VIP. While vestibular tuning recalibrated in line with vestibular perceptual shifts (like MSTd and PIVC), visual tuning recalibrated opposite in direction to the visual perceptual shifts (and opposite in direction to MSTd visual recalibration). These findings indicate that visual responses in VIP do not reflect a simple feed-forward projection from MSTd. They also suggest that visual responses in VIP are not decoded for heading perception (otherwise these would not recalibrate in opposite directions). This interpretation is in

line with findings that inactivation (Chen *et al.*, 2016) and microstimulation (Yu and Gu, 2018) in VIP do not affect perceptual decisions. Thus, the convergence of visual and vestibular signals in VIP likely serves purposes other than cue integration.

The results here also shed new light on the neuronal shifts observed in VIP during supervised recalibration (Zaidel *et al.*, 2017). There, because behavioral responses shifted in the same direction for both cues, it was reasonable to interpret visual and vestibular tuning shifts in accordance with their corresponding cue shifts. However, the results here indicate that yoking of visual and vestibular tuning is observed in VIP irrespective of the paradigm (supervised or unsupervised). Hence yoked recalibration is a feature of VIP, not just supervised recalibration.

We previously found strong choice-related activity in VIP neurons (Zaidel *et al.*, 2017). Accordingly, we considered that shifts in VIP neuronal tuning (during supervised calibration) might simply reflect the altered choices (Zaidel *et al.*, 2021). However, choice-related activity cannot explain the results here, because the predicted shifts in neuronal tuning would be in the same direction as the altered choices (behavioral shifts), whereas we found contrary visual recalibration. To understand contrary shifts that could arise despite strong choice-related activity in VIP, we investigated choice tuning in VIP neurons. We found that choice tuning in VIP decreased during unsupervised calibration. This allowed contrary shifts to be exposed. It also opens up new and fascinating questions regarding the purpose of contrary visual recalibration in VIP.

Because visual and vestibular tuning in VIP both shifted in the same direction (in

accordance with vestibular behavioral shifts) we speculate that VIP recalibration reflects a global shift in the reference frame, following vestibular recalibration. This notion is consistent with suggestions that VIP encodes self-motion in head or body-centered coordinates (Chen et al., 2013b; 2018; Zhang et al., 2004). Accordingly, visual responses in VIP are transformed into a vestibular-recalibrated space. This leads to a remarkable dissociation between visual tuning in VIP and MSTd. Interestingly, visual self-motion perception follows the MSTd (not VIP) recalibration. This is in line with a causal connection between MSTd and visual heading discrimination (Britten and van Wezel, 1998; Gu *et al.*, 2012). What purpose might such visual signals in VIP serve? One possible idea is that they might reflect an expectation signal – e.g., predicted vestibular or somatosensory sensation, based on the current visual signal. During combined stimuli (in the recalibration and post-calibration blocks), the visual signal always appeared together with the vestibular sensory input. Thus, if visual responses in VIP reflect vestibular expectations, then these would shift together with vestibular (rather than visual) recalibration.

Limitations and future directions

Our results revealed correlations between neuronal recalibration and cross-sensory behavioral recalibration. However, they do not implicate any causal connections. Therefore, whether these cortical areas are actively involved in cross-sensory recalibration, vs. simply reflecting the recalibrated signals, requires further research. To probe more directly for causal links, direct manipulation of

neuronal activity might be required. For example, would reversible inactivation or microstimulation (of one or a combination of these multisensory areas) eliminate (or bias) unsupervised recalibration? In addition, future studies are needed to examine how the systematic error between vestibular and visual heading signals is detected. This likely involves additional brain areas, for example, the cerebellum, implicated in internal-model-based error monitoring (Markov et al., 2021; Rondi-Reig et al., 2014), and/or the Anterior Cingulate Cortex (ACC), implicated in conflict monitoring (Bush et al., 2000; Holroyd and Coles, 2002). Thus, a wide-ranging effort to record and manipulate neural activity across a variety of brain regions will be necessary to tease apart the circuitry underlying this complex and important function.

The most surprising and intriguing finding in this study was the contrary recalibration of visual tuning in VIP. We propose that yoked recalibration of visual and vestibular responses in VIP (despite differential behavioral recalibration) might reflect a global shift in vestibular space. Accordingly, we suggest that visual responses in VIP might reflect an expectation signal (in vestibular space), e.g., a simulation of the expected corresponding vestibular response (or integrated position, because VIP responses are sustained beyond the stimulus period). However, this idea is speculative, and the data from this study cannot address this question. Hence, further research is needed to investigate this idea, for example, by conditioning expectations for vestibular motion on other (non-motion) cues, and investigating whether these cues can induce simulated vestibular responses. If this hypothesis turns out to be true, it could greatly contribute to our understanding regarding the functions of the parietal

555 cortex, and the brain mechanisms of perceptual inference.

556 **Concluding remarks**

557 This study exposed individualized (sensory-specific) recalibration of neuronal
558 signals, resulting from a cross-sensory (visual-vestibular) cue conflict. It further
559 revealed profound differences in neuronal recalibration across multisensory cortical
560 areas MSTd, PIVC and VIP. The results therefore provide novel insights into adult
561 multisensory plasticity, and deepen our understanding regarding the different
562 functions of these multisensory cortical areas.

563 **Methods**

564 ***Subjects and surgery***.

565 Three male rhesus monkeys (*Macaca mulatta*, monkeys D, B, and K) weighing
566 8–10 kg participated in the experiment. Monkeys were first trained to sit in a custom
567 primate chair and gradually exposed to the laboratory environment. Then they
568 chronically implanted a head-restraint cap and a sclera coil for measuring eye
569 movement. After full recovery, monkeys were trained to perform experimental tasks.
570 All animal surgeries and experimental procedures were approved by the Institutional
571 Animal Care and Use Committee at East China Normal University (IACUC protocol
572 number: Mo20200101).

573 ***Equipment setup and motion stimuli***

574 During the experiments, monkeys were head-fixed and seated in a primate chair
575 which was secured to a six-degree of freedom motion platform (Moog, East Aurora,
576 NY, USA; MB-E-6DOF/12/1000Kg). The chair was also inside the magnetic field coil
577 frame (Crist Instrument Co., Inc., Hagerstown, MD, USA) mounted on the platform for
578 measuring eye movement with the sclera coil technique (for details, see Zhao et al.,
579 2021).

580 Vestibular stimuli were delivered by the motion platform (for details, see Gu et al.,
581 2006; Chen et al., 2013; Zhao et al., 2021). Visual stimuli were presented on a large
582 computer screen (Philips BDL4225E, Royal Philips, Amsterdam, Netherlands),
583 attached to the field coil frame. The display (62.5 cm $\times$ 51.5 cm) was viewed from a
584 distance of 43 cm, thus subtending a visual angle of 72° $\times$ 62°. The sides of the coil
585 frame were covered with a black enclosure, so the monkey could only see the visual
586 stimuli on the screen (Gu *et al.*, 2006; Zhao et al., 2021). The display had a pixel
587 resolution of 1920 x 1080 and was updated at 60 Hz. Visual stimuli were programmed
588 in OpenGL to simulate self-motion through a 3D cloud of “stars” that occupied a virtual
589 cube space 80 cm wide, 80 cm tall, and 80 cm deep centered on the central point on
590 the screen. The random-dot density was 0.01/cm^3 (each “star” comprised a triangle
591 with base by height: 0.15 cm $\times$ 0.15 cm). Monkeys wore custom stereo glasses made
592 from Wratten filters (red #29 and green #61; Barrington, NJ, USA), such that the optic
593 flow stimuli could be rendered in three dimensions as red-green anaglyphs.

The self-motion stimulus was either vestibular-only, visual-only, or combined (visual and vestibular stimuli). In the vestibular-only condition, there was no optical flow on the screen and the monkey was translated by the motion platform. In the visual-only condition, the motion platform remained stationary while the optic flow was presented on the screen. For the combined condition, the monkey experienced both translation motion and optic flow simultaneously. Each stimulus motion followed a Gaussian profile with a duration of 1 s, and an amplitude of 13 cm (bottom row, **Fig. 6**). The peak velocity was 0.41 m/s, and the peak acceleration was 2.0 m/s^2.

Task and recalibration protocol

The monkeys were trained to report their direction of translation with a two-alternative forced-choice (2AFC) heading discrimination task (for details, see Gu et al., 2008; Chen et al., 2013). In each trial, the monkey experienced a primarily forward motion with a small leftward or rightward component. During stimulation, the animal was required to maintain fixation on a central point within a 3° × 3° window. At the end of the trial (after a 300ms delay period beyond the end of the stimulus), the monkeys needed to make a saccade to one of two choice targets (located 5° to the left and right of the central fixation point) to report their perceived motion as leftward or rightward relative to straight ahead. The saccade endpoint had to remain within 2.5° of the target for at least 150 ms to be considered a valid choice. Correct responses were rewarded with a drop of liquid.

To elicit recalibration, we used a similar unsupervised cue-conflict recalibration

615 protocol previously tested behaviorally in humans and monkeys (Zaidel *et al.*, 2011).
616 Each experimental session consisted of three consecutive blocks, as described here
617 below.

618 ***Pre-recalibration block***. This block was used to deduce the baseline
619 performance (psychometric curve) of each modality for the monkeys, thus only a
620 single cue (vestibular-only or visual-only) stimulus was presented (**Fig. 1A**). Across
621 trials, the heading angle was varied in small steps around straight ahead. Ten
622 logarithmically spaced heading angles were tested for each monkey (±16°, ±8°, ±4°,
623 ±2°, and ±1°). To get monkeys accustomed to not getting a reward for all the trials, we
624 rewarded the monkeys with a 95% probability for correct choices and didn't reward
625 them for incorrect choices.

626 ***Recalibration block*.** Only combined vestibular-visual cues were presented in
627 this block (**Fig. 1B**). There was a discrepancy (Δ) between the vestibular and visual
628 cues, which was introduced gradually from ± 2° to ± 10° with steps of 2°, and then
629 held at ± 10° for the rest of the block. This gradual introduction was designed to
630 prevent monkeys from realizing the discrepancy. The sign of Δ represents the
631 orientation of discrepancy: positive Δ (i.e. Δ^+) indicates vestibular cue to the right and
632 visual cue to the left, and vice versa for negative Δ (i.e. Δ^-). Every session used only
633 one sign, positive or negative. The combined cue heading was defined as the
634 midpoint between the vestibular and visual headings, such that each (vestibular/visual)
635 heading was offset to the right and left (or left and right) in relation to the combined
636 heading. The same ten heading angles as in the pre-recalibration block were used.

637 Unlike the pre-recalibration block, monkeys only needed to maintain fixation on the
638 central point during the stimulus presentation and didn't need to make choices at the
639 end of trials. They were rewarded for all the trials for which they maintained fixation.
640 7~10 repetitions were run for each Δ increment, and an additional 10~16 repetitions
641 were run for maximum Δ (±10°).

642 ***Post-recalibration block***. During this block, performance of the individual
643 (visual/vestibular) modalities was once again tested using single modality trials (as in
644 the pre-recalibration block). Responses to these trials were used to measure
645 recalibration. The single cue trials were interleaved with combined-cue trials (with a
646 10° discrepancy, like the end of the recalibration block, **Fig. 1C**). The combined cue
647 trials were interleaved to maintain the recalibration while it was measured (for details,
648 see Zaidel et al., 2011). To avoid perturbing the recalibrated behavior, we adjusted the
649 reward probability for single-cue trials as follows: if the single cue heading was of
650 relatively large magnitude, such that, if it were part of a combined cue trial also the
651 other cue would lie to the same side (right or left), monkeys were rewarded as in the
652 pre-recalibration block (95% probability reward for correct choices; no reward for
653 incorrect choices). If, however, the heading for other modality would have been to the
654 opposite side, the monkeys were rewarded stochastically (70% reward probability,
655 regardless of their choices).

656 ***Electrophysiological recordings***

657 We recorded extracellular activity from isolated single neurons in areas MSTd,

PIVC, and VIP using tungsten microelectrodes (Frederick Haer Company, Bowdoin, ME, USA; tip diameter ~3 μm; impedance, 1~2 MΩ at 1 kHz). The microelectrode was advanced into the cortex through a transdural guide tube, using a hydraulic microdrive (Frederick Haer Company). Raw neural signals were amplified, band-pass filtered (400–5000 Hz), and digitized at 25 kHz using the AlphaOmega system (AlphaOmega Instruments, Nazareth Illit, Israel). The spike times sorted online along with all behavioral events were collected with 1 ms resolution using the Tempo system for offline analysis. If the online sorting was not adequate, offline spike sorting was performed.

The target areas (VIP, PIVC, and MSTd) were identified based on the patterns of gray and white matter transitions, magnetic resonance imaging (MRI) scans, stereotaxic coordinates, and physiological response properties as described previously (MSTd: Gu et al., 2006; PIVC: Chen et al., 2010; VIP: Chen et al., 2011).

Data analysis

Data analysis was performed with custom scripts in Matlab R2016a (The MathWorks, Natick, MA, USA). Psychometric function plots were constructed by plotting the proportion of “rightward” choices as a function of heading angle and then fitted with a cumulative Gaussian distribution function using the *psignifit* toolbox for MATLAB (version 2.5.6). For each experimental session, separate psychometric functions were constructed for visual and vestibular conditions before and after recalibration. The psychophysical threshold and point of subjective equality (PSE)

were defined as the SD (σ) and mean (μ), respectively, deduced from the best-fitting function. The PSE represents the heading angle of equal right/left choice proportion, i.e., perceived straight ahead, also known as the bias. The vestibular/visual recalibration effect was calculated for each session by subtracting the PSE value of the pre-recalibration from that of the post-recalibration PSE.

Neuronal heading tuning curves were constructed (pre/post recalibration block and vestibular/visual cue) by computing the average FR (in units of spikes/s, the baseline FRs subtracted) for each heading over the stimulus presentation (t=0-1s). A neuron was considered tuned to vestibular or visual cue if the linear regression of FR vs. heading (over the narrow range -16° to 16°) had a significant slope ($p < 0.05$, Pearson's correlation). When calculating the group effects of recalibration for a vestibular or visual cue, we only considered cells with significant tuning either pre- or post-recalibration. This resulted in 49 and 66 (of 118 recorded) VIP neurons tuned to vestibular and visual cues, respectively (31 of which were tuned to both); 60 (of 160 recorded) PIVC neurons tuned to vestibular cues; 23 and 65 (of 83 recorded) MSTd neurons tuned to vestibular and visual cues, respectively.

To estimate neural recalibration (for comparison to behavioral recalibration) we constructed neurometric functions (Chen *et al.*, 2013a; Fetsch *et al.*, 2012; Gu *et al.*, 2008; Gu *et al.*, 2007) for the pre-recalibration and post-recalibration data (each calculated after subtracting the mean baseline firing rate respectively). Specifically, both the pre-recalibration and post-recalibration data were normalized (z-scored) by subtracting the pre-recalibration mean response and dividing by the pre-recalibration

SD across stimulus repetitions. Then ROC (receiver operating characteristic) analysis was used to compute the ability of an ideal observer to discriminate between the z-scored responses (for each heading) and 0° (straight ahead). These ROC values were fitted with a cumulative Gaussian function (like for behavioral psychometrics), and neuronal recalibration was measured by the difference in PSE (as done for behavior).

To assess neuronal recalibration at different time points during the stimulus, we calculated response metrics in 200 ms time windows, starting at stimulus onset, and shifted in steps of 100 ms. The time index (the center of the window) ranged from t = 0.1 s to t = 1.2 s (relative to stimulus onset). This range did not include the saccade, which could only take place after t = 1.3 s because of the delay period (300ms) that was at the end of the stimulus.

Partial correlation analysis

To disassociate the unique contributions of heading stimuli and choices to the neural responses (FRs), we computed Pearson partial correlations between these variables (for details, see Zaidel et al., 2017; Chen et al., 2021). This produced a heading partial correlation, R_h, that captured the linear relationship between firing rate (FR) and heading (H) given the monkey's choice (C), as well as a choice partial correlation, R_c, that captured the relationship between firing rate and choice given the stimulus heading. Partial correlations were calculated over the entire 1 s stimulus duration. Positive heading partial correlations indicate that firing rates were greater for

722 rightward than leftward headings (given the choices). Likewise, positive choice partial
723 correlations indicate that firing rates were greater for choices made to the right than
724 choices made to the left (given the stimulus headings).

725 ***Statistical Analysis***

726 To evaluate differences in monkeys' behavior (PSE), heading, or choice partial
727 correlations, between pre- and post-recalibration, we used paired t-tests. Possible
728 differences in spontaneous (baseline) firing rates between pre- and post-recalibration
729 were evaluated using Bayesian paired-samples t-tests (BF_{10} values). Statistical
730 analysis was conducted using the open-source statistical software program JASP
731 (Version 0.16.3).

732 **Acknowledgments:** This work was supported by grants from the "technology innovation
733 2030--major projects" on brain science and brain-like computing of the Ministry of Science
734 and Technology of China (No. 2021ZD0202600), the National Basic Research Program of
735 China (No. 32171034) to A.C., and the ISF-NSFC joint research program to A.C. (No.
736 32061143003) and A.Z. (No. 3318/20). We thank Prof. Dora Angelaki for the helpful
737 comments. We are also grateful to Minhu Chen for outstanding computer programming.

738 **Competing interests**

739 Authors declare no competing interests.

740 **Data and Code availability statement**

741 The data and analysis code for this study have been uploaded to github and can be

742 found at https://github.com/FuZengBio/Recalibration.

743 **Additional files**

744 Supplementary files

745 **References**

746 Abdulkarim, Z., Hayatou, Z., and Ehrsson, H.H. (2021). Sustained rubber hand illusion after the
747 end of visuotactile stimulation with a similar time course for the reduction of subjective ownership
748 and proprioceptive drift. Experimental brain research *239*, 3471-3486.

749 Atkins, J.E., Jacobs, R.A., and Knill, D.C. (2003). Experience-dependent visual cue recalibration
750 based on discrepancies between visual and haptic percepts. Vision research *43*, 2603-2613.

751 Bertelson, P., and De Gelder, B. (2004). The psychology of multimodal perception. Crossmodal
752 space and crossmodal attention, 141-177.

753 Botvinick, M., and Cohen, J. (1998). Rubber hands 'feel'touch that eyes see. Nature *391*, 756-756.

754 Brainard, M.S., and Knudsen, E.I. (1993). Experience-dependent plasticity in the inferior colliculus:
755 a site for visual calibration of the neural representation of auditory space in the barn owl. Journal
756 of Neuroscience *13*, 4589-4608.

757 Bremmer, F., Klam, F., Duhamel, J.R., Ben Hamed, S., and Graf, W. (2002). Visual–vestibular
758 interactive responses in the macaque ventral intraparietal area (VIP). European Journal of
759 Neuroscience *16*, 1569-1586.

760 Britten, K.H. (2008). Mechanisms of self-motion perception. Annu. Rev. Neurosci. *31*, 389-410.

761 Britten, K.H., and van Wezel, R.J. (1998). Electrical microstimulation of cortical area MST biases
762 heading perception in monkeys. Nature neuroscience *1*, 59-63.

763 Britten, K.H., and Van Wezel, R.J. (2002). Area MST and heading perception in macaque monkeys.
764 Cerebral cortex *12*, 692-701.

765 Burge, J., Ernst, M.O., and Banks, M.S. (2008). The statistical determinants of adaptation rate in
766 human reaching. Journal of vision *8*, 20-20.

767 Burge, J., Girshick, A.R., and Banks, M.S. (2010). Visual–haptic adaptation is determined by relative
768 reliability. Journal of Neuroscience *30*, 7714-7721.

769 Bush, G., Luu, P., and Posner, M.I. (2000). Cognitive and emotional influences in anterior cingulate
770 cortex. Trends in cognitive sciences *4*, 215-222.

771 Butler, J.S., Campos, J.L., and Bülthoff, H.H. (2015). Optimal visual–vestibular integration under
772 conditions of conflicting intersensory motion profiles. Experimental brain research *233*, 587-597.

773 Butler, J.S., Smith, S.T., Campos, J.L., and Bülthoff, H.H. (2010). Bayesian integration of visual and
774 vestibular signals for heading. Journal of vision *10*, 23-23.

775 Canon, L.K. (1970). Intermodality inconsistency of input and directed attention as determinants of
776 the nature of adaptation. Journal of experimental psychology *84*, 141.

777 Chen, A., DeAngelis, G.C., and Angelaki, D.E. (2010). Macaque parieto-insular vestibular cortex:
778 responses to self-motion and optic flow. Journal of Neuroscience *30*, 3022-3042.

779 Chen, A., DeAngelis, G.C., and Angelaki, D.E. (2011a). A comparison of vestibular spatiotemporal
780 tuning in macaque parietoinsular vestibular cortex, ventral intraparietal area, and medial superior
781 temporal area. Journal of Neuroscience *31*, 3082-3094.

782 Chen, A., DeAngelis, G.C., and Angelaki, D.E. (2011b). Representation of vestibular and visual cues
783 to self-motion in ventral intraparietal cortex. Journal of Neuroscience *31*, 12036-12052.

784 Chen, A., DeAngelis, G.C., and Angelaki, D.E. (2013a). Functional specializations of the ventral
785 intraparietal area for multisensory heading discrimination. Journal of Neuroscience *33*,
786 3567-3581.

787 Chen, A., Gu, Y., Liu, S., DeAngelis, G.C., and Angelaki, D.E. (2016). Evidence for a causal
788 contribution of macaque vestibular, but not intraparietal, cortex to heading perception. Journal of

789 Neuroscience *36*, 3789-3798.

790 Chen, A., Zeng, F., DeAngelis, G.C., and Angelaki, D.E. (2021). Dynamics of heading and

791 choice-related signals in the parieto-insular vestibular cortex of macaque monkeys. Journal of

792 Neuroscience *41*, 3254-3265.

793 Chen, X., DeAngelis, G.C., and Angelaki, D.E. (2013b). Diverse spatial reference frames of

794 vestibular signals in parietal cortex. Neuron *80*, 1310-1321.

795 Chen, X., DeAngelis, G.C., and Angelaki, D.E. (2018). Flexible egocentric and allocentric

796 representations of heading signals in parietal cortex. Proceedings of the National Academy of

797 Sciences *115*, E3305-E3312.

798 Colby, C.L., Duhamel, J.-R., and Goldberg, M.E. (1993). Ventral intraparietal area of the macaque:

799 anatomic location and visual response properties. Journal of neurophysiology *69*, 902-914.

800 de Winkel, K.N., Weesie, J., Werkhoven, P.J., and Groen, E.L. (2010). Integration of visual and

801 inertial cues in perceived heading of self-motion. Journal of vision *10*, 1-1.

802 Dokka, K., DeAngelis, G.C., and Angelaki, D.E. (2015). Multisensory integration of visual and

803 vestibular signals improves heading discrimination in the presence of a moving object. Journal of

804 Neuroscience *35*, 13599-13607.

805 Duffy, C.J., and Wurtz, R.H. (1995). Response of monkey MST neurons to optic flow stimuli with

806 shifted centers of motion. Journal of Neuroscience *15*, 5192-5208.

807 Duhamel, J.-R., Colby, C.L., and Goldberg, M.E. (1998). Ventral intraparietal area of the macaque:

808 congruent visual and somatic response properties. Journal of neurophysiology *79*, 126-136.

809 Ernst, M.O., and Banks, M.S. (2002). Humans integrate visual and haptic information in a

810 statistically optimal fashion. Nature *415*, 429-433.

811 Ernst, M.O., and Bülthoff, H.H. (2004). Merging the senses into a robust percept. Trends in
812 cognitive sciences *8*, 162-169.
813 Ernst, M.O., and Di Luca, M. (2011). Multisensory perception: from integration to remapping.
814 Sensory cue integration, 224-250.
815 Fetsch, C.R., Pouget, A., DeAngelis, G.C., and Angelaki, D.E. (2012). Neural correlates of
816 reliability-based cue weighting during multisensory integration. Nature neuroscience *15*,
817 146-154.
818 Fetsch, C.R., Turner, A.H., DeAngelis, G.C., and Angelaki, D.E. (2009). Dynamic reweighting of
819 visual and vestibular cues during self-motion perception. Journal of Neuroscience *29*,
820 15601-15612.
821 Gu, Y. (2018). Vestibular signals in primate cortex for self-motion perception. Current opinion in
822 neurobiology *52*, 10-17.
823 Gu, Y., Angelaki, D.E., and DeAngelis, G.C. (2008). Neural correlates of multisensory cue
824 integration in macaque MSTd. Nature neuroscience *11*, 1201-1210.
825 Gu, Y., DeAngelis, G.C., and Angelaki, D.E. (2007). A functional link between area MSTd and
826 heading perception based on vestibular signals. Nature neuroscience *10*, 1038-1047.
827 Gu, Y., DeAngelis, G.C., and Angelaki, D.E. (2012). Causal links between dorsal medial superior
828 temporal area neurons and multisensory heading perception. Journal of Neuroscience *32*,
829 2299-2313.
830 Gu, Y., Watkins, P.V., Angelaki, D.E., and DeAngelis, G.C. (2006). Visual and nonvisual contributions
831 to three-dimensional heading selectivity in the medial superior temporal area. Journal of
832 Neuroscience *26*, 73-85.

833 Held, R. (1961). Sensory deprivation: Facts in search of a theory. Exposure-history as a factor in
834 maintaining stability of perception and coordination. Journal of Nervous and Mental disease.
835 Holroyd, C.B., and Coles, M.G. (2002). The neural basis of human error processing: reinforcement
836 learning, dopamine, and the error-related negativity. Psychological review *109*, 679.
837 Kennett, S., Taylor-Clarke, M., and Haggard, P. (2001). Noninformative vision improves the spatial
838 resolution of touch in humans. Current Biology *11*, 1188-1191.
839 Knudsen, E.I. (2002). Instructed learning in the auditory localization pathway of the barn owl.
840 Nature *417*, 322-328.
841 Knudsen, E.I., and Brainard, M.S. (1991). Visual instruction of the neural map of auditory space in
842 the developing optic tectum. Science *253*, 85-87.
843 Kramer, A., Röder, B., and Bruns, P. (2020). Feedback modulates audio-visual spatial recalibration.
844 Frontiers in integrative neuroscience *13*, 74.
845 Lewald, J. (2002). Rapid adaptation to auditory-visual spatial disparity. Learning & Memory *9*,
846 268-278.
847 Linkenhoker, B.A., and Knudsen, E.I. (2002). Incremental training increases the plasticity of the
848 auditory space map in adult barn owls. Nature *419*, 293-296.
849 Markov, D.A., Petrucco, L., Kist, A.M., and Portugues, R. (2021). A cerebellar internal model
850 calibrates a feedback controller involved in sensorimotor control. Nature communications *12*,
851 1-21.
852 Maunsell, J., and van Essen, D.C. (1983). The connections of the middle temporal visual area (MT)
853 and their relationship to a cortical hierarchy in the macaque monkey. Journal of Neuroscience *3*,
854 2563-2586.

855 Oman, C.M. (1990). Motion sickness: a synthesis and evaluation of the sensory conflict theory.
856 Canadian journal of physiology and pharmacology *68*, 294-303.

857 Park, H., and Kayser, C. (2021). The neurophysiological basis of the trial-wise and cumulative
858 ventriloquism aftereffects. Journal of Neuroscience *41*, 1068-1079.

859 Radeau, M., and Bertelson, P. (1974). The after-effects of ventriloquism. The Quarterly journal of
860 experimental psychology *26*, 63-71.

861 Reason, J.T., and Brand, J.J. (1975). Motion sickness (Academic press).

862 Recanzone, G.H. (1998). Rapidly induced auditory plasticity: the ventriloquism aftereffect.
863 Proceedings of the National Academy of Sciences *95*, 869-875.

864 Rock, I., and Victor, J. (1964). Vision and touch: An experimentally created conflict between the
865 two senses. Science *143*, 594-596.

866 Rondi-Reig, L., Paradis, A.-L., Lefort, J.M., Babayan, B.M., and Tobin, C. (2014). How the
867 cerebellum may monitor sensory information for spatial representation. Frontiers in systems
868 neuroscience *8*, 205.

869 Schlack, A., Hoffmann, K.P., and Bremmer, F. (2002). Interaction of linear vestibular and visual
870 stimulation in the macaque ventral intraparietal area (VIP). European Journal of Neuroscience *16*,
871 1877-1886.

872 Schlack, A., Sterbing-D'Angelo, S.J., Hartung, K., Hoffmann, K.-P., and Bremmer, F. (2005).
873 Multisensory space representations in the macaque ventral intraparietal area. Journal of
874 Neuroscience *25*, 4616-4625.

875 Schroeder, C.E., and Foxe, J.J. (2002). The timing and laminar profile of converging inputs to
876 multisensory areas of the macaque neocortex. Cognitive Brain Research *14*, 187-198.

877 Shupak, A., and Gordon, C.R. (2006). Motion sickness: advances in pathogenesis, prediction,
878 prevention, and treatment. Aviation, space, and environmental medicine *77*, 1213-1223.
879 Stein, B.E., Stanford, T.R., and Rowland, B.A. (2014). Development of multisensory integration
880 from the perspective of the individual neuron. Nature Reviews Neuroscience *15*, 520-535.
881 Thériault, R., Landry, M., and Raz, A. (2022). The Rubber Hand Illusion: Top-down attention
882 modulates embodiment. Quarterly Journal of Experimental Psychology, 17470218221078858.
883 Tsakiris, M., and Haggard, P. (2005). The rubber hand illusion revisited: visuotactile integration
884 and self-attribution. Journal of experimental psychology: Human perception and performance *31*,
885 80.
886 Ungerleider, L.G., and Desimone, R. (1986). Cortical connections of visual area MT in the macaque.
887 Journal of Comparative Neurology *248*, 190-222.
888 van Beers, R.J., Wolpert, D.M., and Haggard, P. (2002). When feeling is more important than
889 seeing in sensorimotor adaptation. Current biology *12*, 834-837.
890 Warren, W.H., Morris, M.W., and Kalish, M. (1988). Perception of translational heading from
891 optical flow. Journal of Experimental Psychology: Human Perception and Performance *14*, 646.
892 Watson, D.M., Akeroyd, M.A., Roach, N.W., and Webb, B.S. (2021). Multiple spatial reference
893 frames underpin perceptual recalibration to audio-visual discrepancies. PloS one *16*, e0251827.
894 Webster, M.A. (2012). Evolving concepts of sensory adaptation. F1000 biology reports *4*.
895 Wurtz, R.H., and Duffy, C.J. (1992). Neuronal correlates of optic flow stimulation. Annals of the
896 New York Academy of Sciences *656*, 205-219.
897 Yu, X., and Gu, Y. (2018). Probing sensory readout via combined choice-correlation measures and
898 microstimulation perturbation. Neuron *100*, 715-727. e715.

899 Zaidel, A., DeAngelis, G.C., and Angelaki, D.E. (2017). Decoupled choice-driven and
900 stimulus-related activity in parietal neurons may be misrepresented by choice probabilities.
901 Nature Communications *8*, 1-13.

902 Zaidel, A., Laurens, J., DeAngelis, G.C., and Angelaki, D.E. (2021). Supervised multisensory
903 calibration signals are evident in VIP but not MSTd. Journal of Neuroscience *41*, 10108-10119.

904 Zaidel, A., Ma, W.J., and Angelaki, D.E. (2013). Supervised calibration relies on the multisensory
905 percept. Neuron *80*, 1544-1557.

906 Zaidel, A., Turner, A.H., and Angelaki, D.E. (2011). Multisensory calibration is independent of cue
907 reliability. Journal of Neuroscience *31*, 13949-13962.

908 Zhang, T., Heuer, H.W., and Britten, K.H. (2004). Parietal area VIP neuronal responses to heading
909 stimuli are encoded in head-centered coordinates. Neuron *42*, 993-1001.

910 Zhao, B., Zhang, Y., and Chen, A. (2021). Encoding of vestibular and optic flow cues to self-
911 motion in the posterior superior temporal polysensory area. The Journal of Physiology *599*,
912 3937-3954.

913 Zierul, B., Röder, B., Tempelmann, C., Bruns, P., and Noesselt, T. (2017). The role of auditory cortex
914 in the spatial ventriloquism aftereffect. NeuroImage *162*, 257-268.

Supplementary Material

Contrary neuronal recalibration in different multisensory cortical areas

Fu Zeng[1], Adam Zaidel[2,] * and Aihua Chen[1,] *

1. Key Laboratory of Brain Functional Genomics (Ministry of Education), East China Normal University, 3663 Zhongshan Road N., Shanghai 200062, China
2. Gonda Multidisciplinary Brain Research Center, Bar-Ilan University, Ramat Gan, 5290002, Israel

* Co-corresponding author: ahchen@brain.ecnu.edu.cn (A.C.) or adam.zaidel@biu.ac.il (A.Z.)

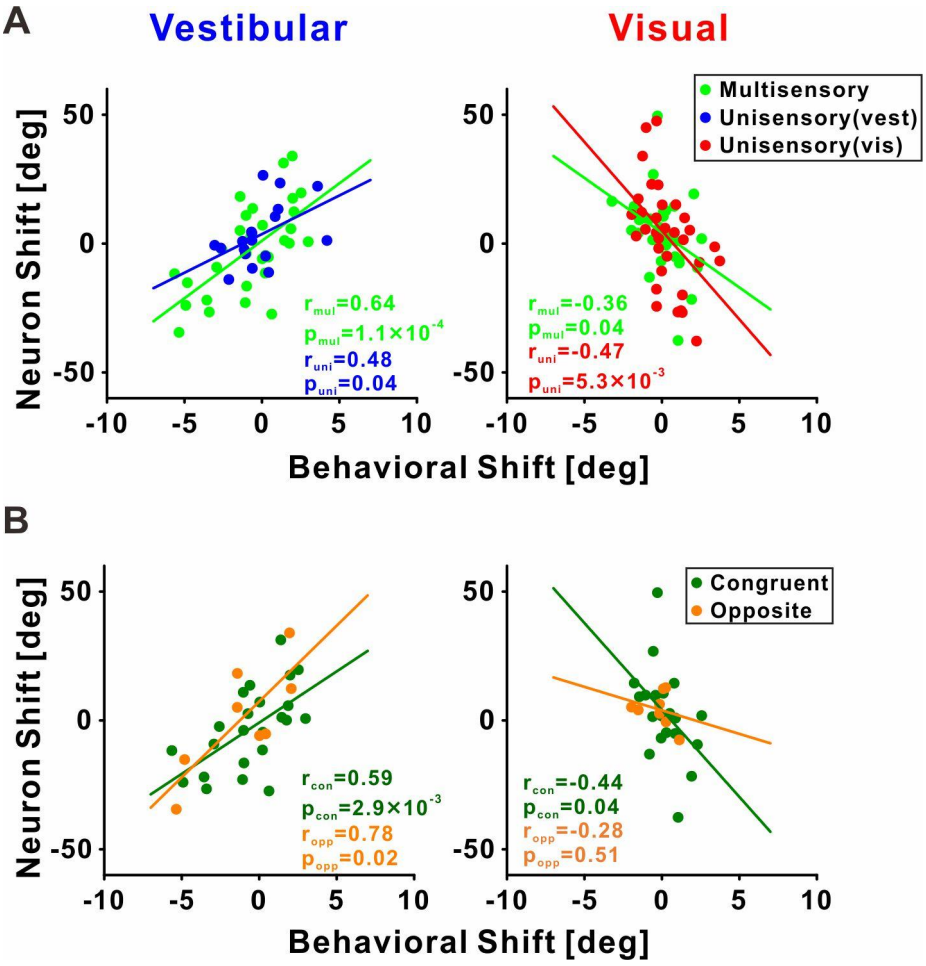

Supplemental Figure 1. **Neuronal vs. behavioral shifts by neuron type in area VIP**. (**A)** Neurons with multisensory (green) and unisensory (blue and red, for vestibular and visual, respectively) tuning. (**B)** Multisensory neurons with congruent, or opposite, vestibular and visual tuning. The neuronal shifts were positively correlated with the behavioral shifts for the vestibular cue (left column), and negatively correlated with the behavioral shifts for the visual cue (right column). Pearson correlation coefficients are presented on the corresponding plots.

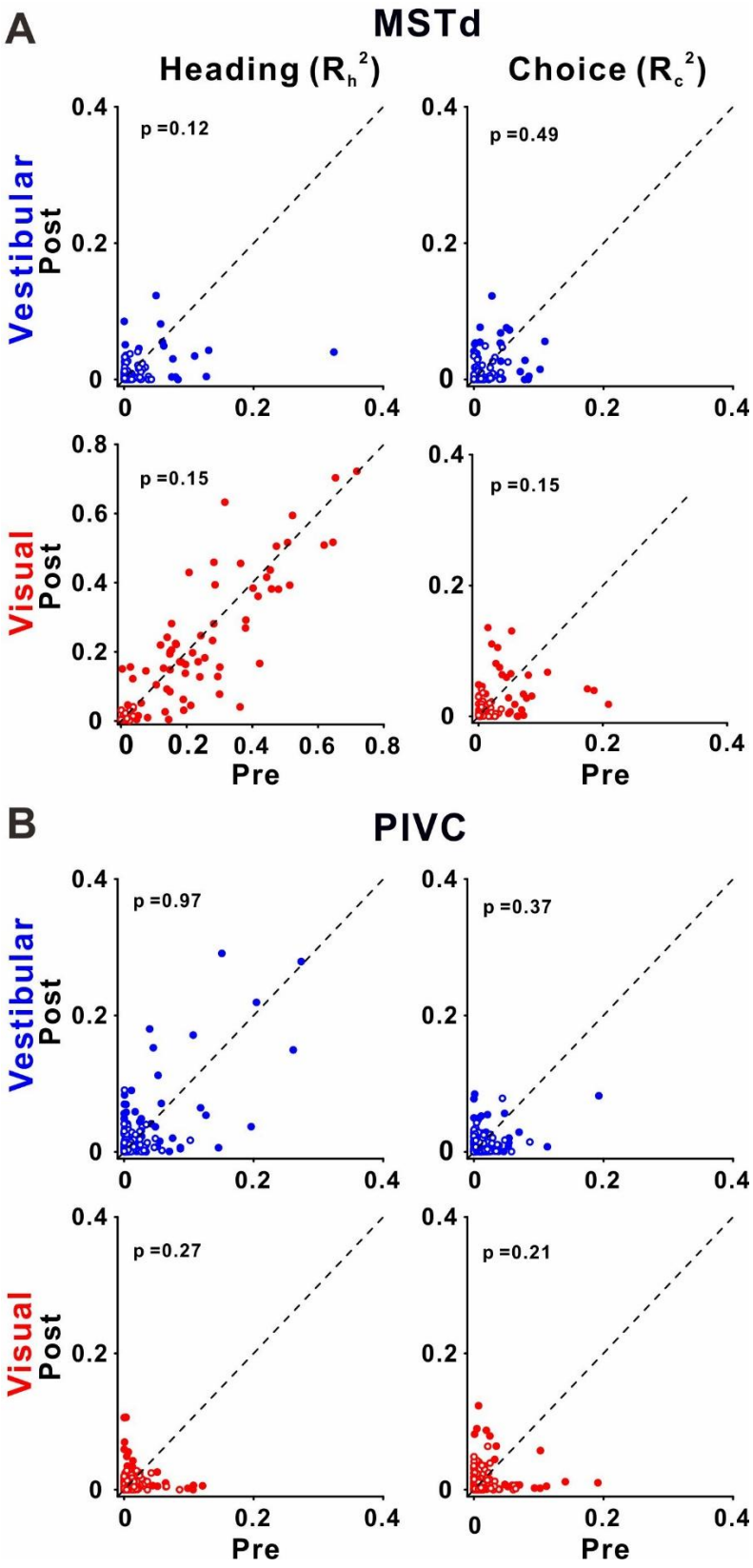

Supplemental Figure 2. **Choice and heading partial correlations in areas MSTd and PIVC**. Plotting conventions are the same as in Figure 8.

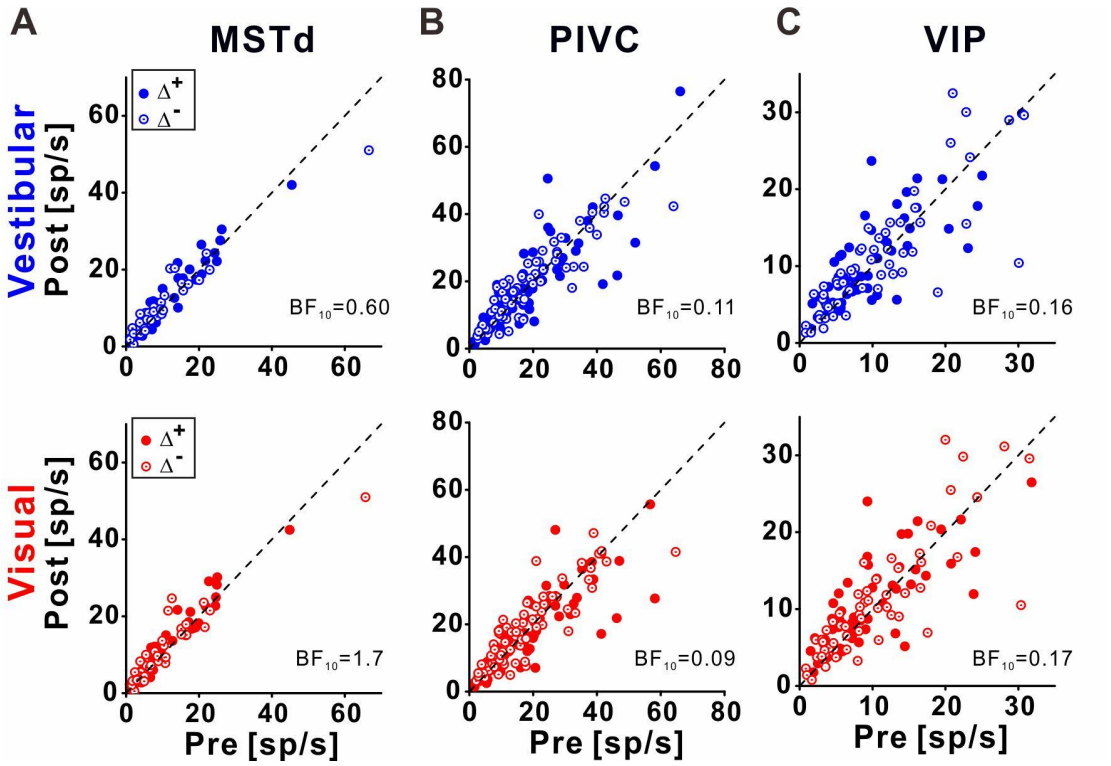

Supplemental Figure 3. **Baseline firing rates in areas MSTd, PIVC and VIP.** The baseline firing rates post- vs. pre-recalibration are plotted for vestibular (upper panel) and visual (bottom panel) cues. Solid symbols represent Δ^+ and open symbols represent Δ^-. Bayes factors (BF_{10}) < ⅓ (as for PIVC and VIP) provide substantial evidence against a change in baseline firing rates. Bayes factors between ⅓ and 3 (as for MSTd) are inconclusive (provide no substantial evidence for, or against, changes).